Environmental Science & Technology

Article

pubs.acs.org/est

First Day of an Oil Spill on the Open Sea: Early Mass Transfers of Hydrocarbons to Air and Water

Jonas Gros,[●,†,‡] Deedar Nabi,[●,†,‡] Birgit Würz,[§] Lukas Y. Wick,[§] Corina P. D. Brussaard,[∥,⊥] Johannes Huisman,[#] Jan R. van der Meer,[▲] Christopher M. Reddy,[○] and J. Samuel Arey*[,†,‡]

[†]Environmental Chemistry Modeling Laboratory (LMCE), GR C2 544, Swiss Federal Institute of Technology at Lausanne (EPFL), Station 2, CH-1015 Lausanne, Switzerland

[‡]Department of Environmental Chemistry, Swiss Federal Institute of Aquatic Science and Technology (Eawag), Überlandstrasse 133, CH-8600 Dübendorf, Switzerland

[§]Department of Environmental Microbiology, Helmholtz Centre for Environmental Research − UFZ, Permoserstrasse 15, D-04318 Leipzig, Germany

[∥]Department of Biological Oceanography, Royal Netherlands Institute for Sea Research (NIOZ), P.O. Box 59, 1790 AB Den Burg, The Netherlands

[⊥]Aquatic Microbiology, Institute for Biodiversity and Ecosystem Dynamics, University of Amsterdam, P.O. Box 94248, 1090 GE Amsterdam, The Netherlands

[#]Response Organisation, RWS Zee&Delta, Postbus 5807, 2280 HV Rijswijk, The Netherlands

[▲]Department of Fundamental Microbiology, Bâtiment Biophore, University of Lausanne, CH-1015 Lausanne, Switzerland

[○]Department of Marine Chemistry & Geochemistry, Woods Hole Oceanographic Institution, Woods Hole, Massachusetts 02543, United States

Supporting Information

ABSTRACT: During the first hours after release of petroleum at sea, crude oil hydrocarbons partition rapidly into air and water. However, limited information is available about very early evaporation and dissolution processes. We report on the composition of the oil slick during the first day after a permitted, unrestrained 4.3 m^3 oil release conducted on the North Sea. Rapid mass transfers of volatile and soluble hydrocarbons were observed, with >50% of $\leq C_{17}$ hydrocarbons disappearing within 25 h from this oil slick of <10 km^2 area and <10 μm thickness. For oil sheen, >50% losses of $\leq C_{16}$ hydrocarbons were observed after 1 h. We developed a mass transfer model to describe the evolution of oil slick chemical composition and water column hydrocarbon concentrations. The model was parametrized based on environmental conditions and hydrocarbon partitioning properties estimated from comprehensive two-dimensional gas chromatography (GC×GC) retention data. The model correctly predicted the observed fractionation of petroleum hydrocarbons in the oil slick resulting from evaporation and dissolution. This is the first report on the broad-spectrum compositional changes in oil during the first day of a spill at the sea surface. Expected outcomes under other environmental conditions are discussed, as well as comparisons to other models.

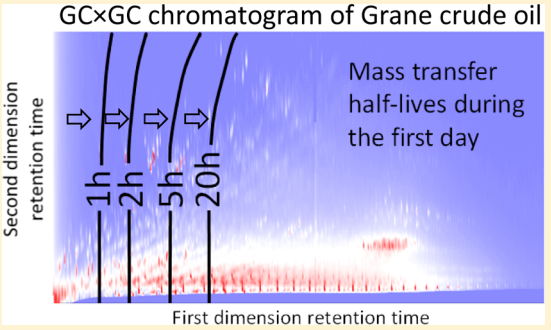

INTRODUCTION

After an oil spill, many petroleum hydrocarbon compounds fractionate rapidly into the atmosphere and water column.[1] The early behavior of oil spilt at sea thus controls the initial exposures of marine organisms to oil components: high concentrations of dissolved aromatic hydrocarbons in the water underlying oil slicks are considered especially likely during the first hours and days after a spill.[2−4]

However, compositional data describing early evaporation and dissolution processes in the field are limited. Environmental sampling does not begin until several days after an accidental oil spill, because logistical challenges preclude early sampling of an unanticipated release. Data describing early fractionations have been reported for long-lasting releases resulting from offshore oil well blowouts[5−8] and natural sea floor oil seeps.[9] However, oil and gas hydrocarbons emitted from the deep sea floor experience prolonged exposure to the water column before reaching the atmosphere at the sea surface. Consequently a deep sea floor release likely undergoes

Received: May 18, 2014
Revised: July 9, 2014
Accepted: July 17, 2014
Published: August 8, 2014

a much greater extent of dissolution compared to a sea surface release. Some experimental data relevant to sea surface releases have been obtained through mesoscale laboratory experiments.[10,11] Additionally, several controlled oil release experiments of up to 100 t have been conducted at sea (off Norway, the United States, Canada, the United Kingdom, and The Netherlands), as early as 1930.[4,12−37] Among these, several studied early evaporation of the slick and/or dispersion/dissolution into the underlying water column,[4,13,17,19,23−27,29,30,32,37] using techniques including the following: evaluation of distillation data for collected oil slick samples; gas chromatography (GC) analysis of slick and water column samples; and in situ fluorimetry, light-scattering, and radioactive tracer tracking of the water column. These field data were used for the development and validation of oil spill models such as the OSCAR model, developed by SINTEF, and its oil weathering model (OWM) component.[15,27,31,33,38] However, limited data is available describing the concentrations of individual hydrocarbons, except a few reports of trends for *n*-alkanes in oil slicks during the initial hours after the release.[4,17,25]

After the release of oil on the sea, several physical processes simultaneously modify oil composition and properties, including evaporation, aqueous dissolution, sorption, emulsification, and dispersion.[1] Evaporation usually dominates the early fractionation of petroleum compounds after a spill, typically affecting compounds with boiling points lower than *n*-pentadecane (*n*-C_{15}).[39] Evaporation can remove up to 75% of the oil volume within a few days for light crude oils, up to 40% for medium crude oils, and about 5% for heavy or residual oils.[40] Under turbulent sea surface conditions, some oils rapidly form water-in-oil emulsions, and this is expected to decrease mass transfer rates.[39,41,42] In this paper the term *mass transfer* has units of mass; the terms *mass transfer rate* or *mass loss rate* have units of mass time^{-1}; and *mass transfer flux* has units of mass time^{-1} area^{-1}.

Compared to evaporation, dissolution removes less mass from the oil phase during early weathering.[4,43−45] However, dissolution is important in terms of aquatic ecotoxicological impact, because several individual soluble hydrocarbon compounds as well as hydrocarbon mixtures are toxic to aquatic species.[1,46−49] For example, total polycyclic aromatic hydrocarbons (PAHs) levels of up to 115 and 42 μg L^{-1} were detected in the water column a few days to months after the *North Cape* and *Exxon Valdez* oil spills, respectively.[50,51] Higher concentrations of total PAHs of up to 100 mg L^{-1} were recorded in the water column during the *Deepwater Horizon* oil spill,[6] where ascending oil and gas were subjected to prolonged exposure to the water column before having the opportunity to ventilate into the atmosphere.[52]

It is challenging to apportion mass transfers of hydrocarbons resulting from evaporation and dissolution out of the oil phase, because both processes act simultaneously on many of the same compounds.[44] Different models have been developed to predict the evaporation and dissolution of hydrocarbons at sea.[4,15,40,43−45,53−69] Several of these models consider oil as a single component,[54−56] unable to capture the independent behaviors of the thousands of compounds that constitute oils.[70] However, models applicable to the partitioning behavior of individual compounds or to pseudocomponents have also been developed.[4,15,43,53,57−69] Additionally, some models consider dispersion, or entrainment of oil into the water column, plus oil dissolution and evaporation.[15,16,62,63,69,71] The processes of evaporation and dispersion have received more extensive field testing,[15,16,19,21,24−26,29,32,37] whereas dissolution has received less evaluation in the field.[12]

Two field studies have evaluated compound-by-compound modeling of evaporation and dissolution for a broad range of petroleum hydrocarbon compounds in beached oils.[43,53] In both studies, comprehensive two-dimensional gas chromatography (GC×GC) retention information was used to estimate the vapor pressures and aqueous solubilities of measured oil hydrocarbons in the *n*-C_{10} to *n*-C_{24} elution range or 174 to 391 °C boiling point range.[72] Resulting estimates of partitioning properties were then used to parametrize simulations of evaporation and dissolution mass transfers for all GC×GC-determined hydrocarbon analytes eluting in this boiling point window. Using this approach, mass transfer model predictions were successfully compared to measured field sample data for oil beached near Cape Cod, MA, after the 2003 *Bouchard 120* oil spill[43] and also for oil beached in San Francisco Bay after the 2007 *Cosco Busan* oil spill.[53] However, neither of these studies evaluated the very early period (<7 days) of mass transfers to air and water.

Here, we report results from a controlled oil release experiment conducted in open waters on the North Sea during September 29−30, 2009. With this study, we aim to bridge the knowledge gap that exists due to the lack of early oil composition data and specifically to shed light on the initial evaporation and dissolution processes during the first day of an oil spill. We present detailed hydrocarbon compositional analysis of collected oil slick and oil sheen samples during the first day after release. These field measurements are compared to a transport model that we developed to describe early mass transfer processes during the field experiment.

EXPERIMENTAL AND COMPUTATIONAL METHODS

Open Sea Oil Spill Experiment. A permitted, controlled oil release experiment was conducted jointly by several European research institutes during September 29−30, 2009, approximately 200 km offshore in the North Sea Netherlands Exclusive Economic Zone. Starting at 12:10 UTC, 4.3 m^3 of Norwegian Grane crude oil was released from the deck of the *Arca*, a hydrographic survey and pollution response vessel, over a 1.15 h period. The resulting unrestrained sea-surface slick was monitored during a 26 h period. The oil had a density of 940 kg m^{-3}, a Reid vapor pressure of 3.4 kPa, and a kinematic viscosity of 373 mm^2 s^{-1} at 20 °C. These and other measured properties of the oil compared favorably with values reported previously by Statoil[73] for Grane crude (Supporting Information Section S-1). Due to weather and logistical constraints, oil slick, oil sheen, and water column samples were taken at irregular time intervals. Oil slick and sheen samples were taken from the sea surface, from a small rubber motorboat deployed from the *Arca*, at several time points after the end of the oil release: 0.58; 0.88; 3.70; 18.07; 19.62; 19.82; 22.53; and 25.23 h. Four water column samples were taken 20 h after the end of the oil release, in three locations, at depth of ∼1.5 m, using a custom-built grab sampler (SI Section S-2). Sampling procedures are described in detail in SI Section S-2. Recorded slick surface area and wind speed measurements during the experiment are given in SI Section S-3.

Analysis of Oil Slick and Oil Sheen Samples. Oil slick and oil sheen samples were analyzed by GC×GC coupled to a flame ionization detector (GC×GC−FID); details of the

analysis method are published elsewhere.[74] GC×GC−FID chromatograms were baseline-corrected with the method of Reichenbach and co-workers[75] using GC Image[76] with the following parameters: 200 deadband pixels per modulation; filter window size of 3 pixels; 3.5 for the expected value of baseline plus noise to the estimated standard deviation of the noise; and one baseline value per modulation. The conservative baseline correction of Reichenbach et al. is appropriate for quantification of the total (resolved plus unresolved) signal.[77] FID response factors of hydrocarbons have been shown to be similar (within ±12% of central value) for 22 PAHs and 16 *n*-alkanes analyzed by GC−FID.[78] Therefore, the GC×GC−FID instrument response factor was assumed to be the same for all hydrocarbon compounds.[77,79] This allowed quantitative comparisons of mass changes of both resolved and unresolved GC×GC-amenable hydrocarbon material between chromatograms of different samples. Collected oil sample chromatograms were then aligned to the neat oil chromatogram.[74]

GC×GC chromatograms were finally normalized so that the total peak volumes of five consecutive *n*-alkanes, octocosane (n-C_{28}) to dotriacontane (n-C_{32}), were of the same magnitude in all chromatograms. These *n*-alkanes were considered unlikely to undergo significant fractionation,[77] and they exhibited relative changes in concentration of ≤15% during the experiment. In order to quantify the peak volumes for these and other individual compounds, we applied the GC Image implementation of the inverted watershed algorithm[76] to the (unaligned) chromatograms, after baseline-correction with the algorithm of Eilers (using lambda $=10^4$ for *n*-alkanes and $10^{6.5}$ for PAHs).[77,80]

Not all petroleum compounds are GC×GC-amenable. Non-GC-amenable compounds include those with very high and very low boiling points that lie outside of the volatility range separated by the instrument, as well as compounds that are thermally unstable or that adhere to active sites within the chromatographic system. The mass contributions of the non-GC-amenable high boiling and low boiling fractions were estimated from true boiling point distillation data for Grane crude provided by Statoil[73] (SI Section S-1). The GC×GC analysis separated an elution range of n-C_9 to n-C_{45}, which corresponds to a simulated distillation boiling point interval of 150 to 550 °C. True distillation data show that 68.9% of the Grane crude oil mass falls within this boiling point window. Consequently we infer that 31.1% of the oil mass was not measured by GC×GC, having point boiling point >550 °C or <150 °C. In this article we will always refer to percentages of the whole oil including the non-GC-amenable fraction. This assumes that the very low-volatility (boiling point >550 °C) compounds remained in the oil phase throughout the duration of the experiment. Several high-volatility compounds, including BTEX (benzene, toluene, ethylbenzene, and xylenes) and n-C_7 to n-C_9 *n*-alkanes, were modeled separately based on their concentrations in neat oil as measured by GC−FID and GC−MS (Table S-3). The remaining 5.6% of oil mass in the <174 °C boiling point range was assumed immediately evaporated upon release, in our model calculations.

Analysis of Water Column Samples. Water column samples were analyzed for several PAHs and *n*-alkanes (n-C_8−n-C_{40}) by gas chromatography coupled to a mass spectrometer (GC−MS) and by headspace GC with a flame ionization detector (GC−FID) for benzene, toluene, ethylbenzene, and xylenes (BTEX). Detailed analysis method descriptions are given in SI Section S-5.

Mass Transfer Model. A transport model was developed to describe mass transfer fluxes of hydrocarbons from floating oil into air and water, as well as downward turbulent mixing of dissolved hydrocarbons in the water column. The model was parametrized based on temperature, wind, and wave conditions observed during the experiment, as well as the observed lateral spreading of the slick detected by SeadarQ radar from the *Arca* and aerial overflight (SI Section S-3). The model was tailored to individual analyzed hydrocarbon compounds based on their known or estimated physical properties, as explained in detail below. None of the model parameters were calibrated based on the observed evolution of hydrocarbon concentration data in either the oil slick or the water column.

The model assumes a well-mixed, uniform layer of oil slick at the sea surface. Oil input to the sea surface was assumed a constant rate during the 1.15 h release period. In the model, the surface area of the oil slick was assumed to grow continuously such that its extent matched the oil slick footprint observed at several time points throughout the experiment (0.98 h before the end of the oil release; and 0.12; 0.93; 1.77; 3.30; 6.37; and 18.27 h after the end of the oil release). The modeled oil slick thickness varied with time and was updated iteratively based on the modeled quantity of total oil slick mass and the observed surface area of the oil slick footprint, assuming a constant oil density. Additionally, the oil slick formed during the field experiment was observed to be patchy, partly interspersed with a visible sheen (thinner oil layer) at the air−water interface. Hence, in the model, oil slick was assumed to cover only half of the footprint, or total sea surface area, explored by the oil spill. Emulsification of the oil in the slick was not visibly noticed during the experiment.

Hydrocarbon mass transfer fluxes (mass time^{-1} area^{-1}) from the liquid oil phase into air and water were computed with a boundary layer model[81]

$$F_{i,oil}|_{evap} = -\frac{C_{i,oil}}{\left(\frac{\delta_{oil}}{D_{i,oil}} + \frac{\delta_{air}}{D_{i,air}\cdot K_{i,a/o}}\right)} \quad (1)$$

$$F_{i,oil}|_{diss} = \frac{\frac{C_{i,water}}{K_{i,w/o}} - C_{i,oil}}{\left(\frac{\delta_{oil}}{D_{i,oil}} + \frac{\delta_{water}}{D_{i,water}\cdot K_{i,w/o}}\right)} \quad (2)$$

where δ_j refers to the boundary layer thickness of phase j, $D_{i,j}$ is the diffusion coefficient of compound i in phase j, $K_{i,j/k}$ is the partition coefficient of compound i between phases j and k, $C_{i,oil}$ is the concentration present in the oil layer, and $C_{i,water}$ is the concentration in the uppermost water layer (1 m thickness). Equations 1 and 2 are comparable to expressions used previously to describe evaporation and dissolution of individual compounds from a liquid oil phase,[4,43,45,57,58,64−69,71] and the correspondences between several of these models are explained in detail in SI Section S-6. Air and water boundary layer thicknesses (δ_{oil} and δ_{water}) were estimated from wind speed.[81] Observed wind speeds ranged from 3 to 4 degrees Beaufort (3.4−7.9 m s^{-1}), and wind speed values used by the model correspond to the middle of the measured Beaufort intervals, with linear interpolation between measurements. Owing to the wind conditions and limited lateral extent of the oil slick, the air phase concentration of hydrocarbons was assumed negligible (zero) for the purposes of estimating evaporative mass transfer fluxes (eq 1).

Vertical turbulent mixing in the water column was modeled with a finite difference formulation, where downward transport was assumed to follow Fick's first law[81−84]

$$F_{i,w}(z)|_{mix} = -E \cdot \frac{\Delta C_{i,w}(z)}{\Delta z_w} \quad (3)$$

where $\Delta C_{i,w}$ is the concentration difference between two water layers for compound i, E is the vertical turbulent mixing coefficient of the water column, and Δz_w is the thickness of the water layers (1 m each). A Neumann boundary condition or wall boundary (vertical concentration gradient equal to zero)[85] was imposed at the sea floor, which had ∼42 m depth.[86] Transport in the water column was assumed to have a vertical gradient only; i.e., dissolved hydrocarbons were assumed to be laterally well-mixed under the oil slick footprint but not extend laterally outside of the slick footprint. Based on an estimated lateral turbulent mixing coefficient of 50−250 $m^2\ s^{-1}$,[81,84] the water mass below the slick was expected to mix 3−7 km laterally over the duration of the experiment. This is similar to the observed oil slick spreading extent of 1.4 km width and 5.2 km length. Therefore, the assumption that hydrocarbons were laterally well-mixed below the oil slick was assumed valid for this early phase of the oil spill. Volatilization of dissolved compounds from the "slick free" water surface (where sheen might be observed) was modeled using previously developed expressions for air−water mass transfer fluxes.[81]

Methods to estimate the vertical turbulent mixing coefficient of the water column based on wind speed have been reported, some of them in an oil spill modeling context.[87−90] However, these formulas neglect convective mixing, which may be dominant at night or in autumn and winter. Therefore, we estimated the air-sea heat flux balance during the experiment, based on wind speed, relative humidity, and air and water temperatures at K13 platform obtained from the Royal Netherlands Meteorological Institute (KNMI).[84,91−93] From these data, we interpreted that convection was the dominant mixing process in the water column throughout the entire duration of the experiment (SI Section S-7). Consistent with a convective mixing situation, we assumed a single mixed layer throughout the entire 42 m depth water column, based on literature reports describing the absence of pycnocline for nearby locations around this time of year.[94,95] Based on the net heat flux, we thus estimated the vertical turbulent mixing coefficient, E, to be 0.22 $m^2\ s^{-1}$ throughout the water column during the entire period of the experiment (see SI Section S-7), using the expression[84]

$$E = k \cdot \left(\frac{\alpha \cdot g \cdot h \cdot H}{C_p \cdot \rho_w} \right)^{1/3} \cdot h \quad (4)$$

where α is the thermal expansivity of water, h is the water depth (∼42 m), H is the net heat flux (SI Figure S-5), C_p is the specific heat capacity of water at constant pressure, ρ_w is the water density, and k is a factor approximately equal to 0.5.[96]

Mass transfer fluxes of oil hydrocarbon compounds more volatile than *n*-decane were modeled individually. For these compounds, partitioning from oil to air and water were estimated based on Raoult's law[81] using experimental vapor pressure and aqueous solubility data.[81,97] Aqueous solubilities were corrected for salinity by dividing by a factor of 1.36.[98] Molecular diffusion constants in air and water were estimated from molar mass and corrected for temperature.[81] Partitioning properties and molar masses for hydrocarbons eluting between *n*-C_{10} and *n*-C_{24} were estimated from GC×GC retention time information (SI Section S-8).[43,72] This includes intervening *n*-alkanes and other substituted aliphatic and aromatic hydrocarbons in the *n*-C_{10}−*n*-C_{24} elution window or boiling point range of 174 to 391 °C. For both individually modeled compounds and GC×GC-analyzed hydrocarbons, estimated or experimental vapor pressure data at 25 °C were temperature-corrected to the surface water temperature of the field site, using enthalpy of vaporization estimates[72,81] or data.[72,97] Surface water temperature was estimated to be 16.1 °C based on measurements at nearby locations (K13 platform and Europlatform). GC×GC-based estimates of aqueous solubility may or may not be valid for *n*-alkanes longer than *n*-C_{11}, due to possible folding of straight-chained *n*-alkanes in aqueous solution,[99] an interpretation that is challenged by recent modeling results.[100] The oil molar volume (0.25 L mol^{-1}) was estimated from the mass-weighted average of the molar mass divided by the measured oil density. Compounds with boiling points >391 °C (corresponding to >*n*-C_{24}) were assumed unaffected by either dissolution or evaporation during the time frame of this experiment.

According to our model, mass transfer fluxes were not limited by molecular diffusion within the oil slick layer, but this process was nevertheless included in the model. Oil-side diffusion limitation of mass transfer fluxes is likely to be important for water-in-oil emulsions,[39,41,42] which were not observed during our experiment. $D_{i,oil}$ was estimated from molecular radius, oil viscosity, and temperature according to the Stokes−Einstein relation.[43,81] Effective compound molecular radii were estimated from molar volume, assuming spherical molecule shape.[53] Oil viscosity was adjusted as a function of temperature (SI equation ES-22)[101] and of the fraction evaporated,[102] using a value of 5 for the "prefactor"; this value lies in between the value of 1 suggested for gasoline and the value of 10 used by Arey et al. for heavy fuel oil.[43]

Dispersion, or oil-in-water emulsion, is the process of entrainment of oil droplets within the water column. Dispersed droplets reduce the amount of oil present within the oil slick and also enhance the rate of hydrocarbon dissolution. Most oil entrainment models are based on the work by Delvigne and Sweeney,[103] which is designed for entrainment by breaking waves.[104] The ADIOS model,[63] which is based on Delvigne and Sweeney's oil entrainment model, predicted 0.7% dispersion during the experiment (SI Section S-9). We estimated that 0.7% dispersion would increase truly dissolved concentrations of the most soluble PAHs by <20%; therefore, we chose not to include this process explicitly in the mass transfer model of our experiment.

We did not conduct a formal error propagation analysis based on model input parameter variability, because we judged that the most important uncertainties arose from the treatment of oil entrainment into the water column, the associated oil−water interactions, and water mass mixing controlled by water column stability. We briefly discuss the sensitivity of the model to these and other uncertainties in the Results and Discussion.

RESULTS AND DISCUSSION

Compositional Changes in Oil Slick and Oil Sheen Samples. Analysis of collected oil slick samples shows that volatile and/or soluble hydrocarbon compounds are removed rapidly from the floating oil during the first day of the oil spill, including several light *n*-alkanes and PAHs (Figure 1). Oil slick

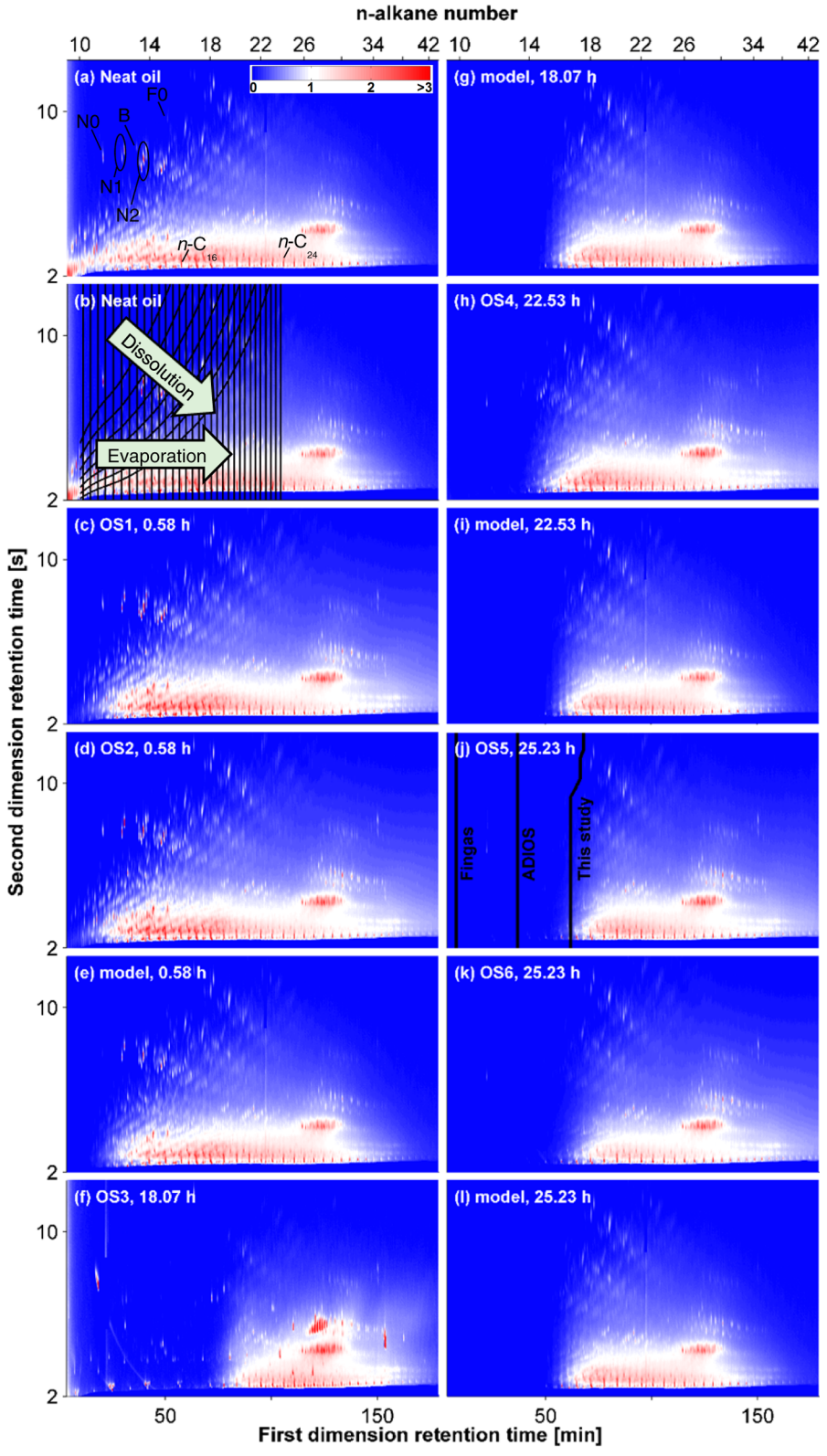

Figure 1. GC×GC−FID chromatograms of oil slick samples, and transport model-generated chromatograms at corresponding times, for (a) neat oil overlaid with positions of selected compounds, including naphthalene (N_0), C_1-naphthalenes (N_1), C_2-naphthalenes (N_2), biphenyl (B), fluorene (F_0), hexadecane (n-C_{16}), and tetracosane (n-C_{24}); (b) neat oil overlaid with solubility and vapor pressure contours; these contours define discrete cells that were used to construct mass loss tables (MLTs); (c) sample OS1; (d) OS2; (e) model (0.58 h); (f) OS3; (g) model (18.07 h); (h) OS4; (i) model (22.53 h); (j) OS5 overlaid with removal extent predictions inferred from Fingas formula ES-16 and the ADIOS model, and the half-life contour predicted by our model; (k) OS6; and (l) model (25.23 h). GC×GC chromatograms are normalized such that the total peak volumes of the five n-alkanes n-C_{28} to n-C_{32} are the same in all chromatograms. Listed time points correspond to time after the end of the oil release. The color scale on the upper right of the neat oil chromatogram indicates FID signal response (arbitrary units).

dx.doi.org/10.1021/es502437e | Environ. Sci. Technol. 2014, 48, 9400−9411

samples OS1 and OS2, taken 0.58 h after the end of the oil release, exhibit 55% ± 9% loss of undecane (n-C_{11}) and 41% ± 10% loss of naphthalene, based on quantification of analyte peak volumes in GC×GC−FID chromatograms (SI Table S-5). Samples OS5 and OS6, taken 25.23 h after the release, exhibited partial to total losses of two- to three-ring PAHs and >50% loss of n-alkanes up to n-C_{17} (SI Table S-5). We did not detect naphthalene in oil slick samples taken after 18 h, in agreement with the transport model and consistent with previous estimates[4] suggesting that naphthalene would disappear from a small sea-surface oil slick within 3 to 8 h after release. Two-ring PAHs are of particular concern for early exposures of organisms in the water column.[1] Normal alkanes and PAHs represent hydrocarbons that are typically evaluated during oil weathering studies. However, n-alkanes and parent PAHs in the n-C_7−n-C_{40} boiling range represent only <2% of the oil mass of Grane crude.

It is more instructive to study the systematic fractionation patterns that arise in GC×GC chromatograms of collected oil slick samples (Figure 1). GC×GC−FID chromatograms allow the visualization and quantification of mass changes affecting all resolved and unresolved hydrocarbon material eluting between n-C_9 and n-C_{45}, corresponding to the 150 to 550 °C boiling point range, which represents 68.9% of the total oil mass. In the oil slick samples, we observe a progressive removal of hydrocarbons that appears initially in the upper left region of the GC×GC chromatogram in early samples and encroaches toward the lower right region of the GC×GC chromatogram with increasing sample age (Figure 1). The observed hydrocarbon fractionation pattern aligns well with plotted contours of estimated liquid vapor pressures of the analyzed hydrocarbons, which decrease progressively from left to right in the GC×GC chromatogram, and plotted contours of estimated aqueous solubilities, which decrease monotonically from upper left to lower right (Figure 1b). The observed removal of both resolved and unresolved hydrocarbon mass from oil slick samples is thus consistent with the expected combined effects of evaporation and dissolution, manifest as a disappearance of hydrocarbons systematically from the upper left to the lower right of the GC×GC chromatogram.

Mass transfer model simulations of oil slick evolution can be projected directly on the GC×GC chromatogram of the neat oil,[43] enabling the visualization of simulated oil slick sample chromatograms throughout the duration of the field experiment (Figure 1). The mass transfer model predicts that hydrocarbon material removal corresponds to a progressive disappearance of compounds from upper left to lower right in the GC×GC chromatogram. On visual inspection, the mass transfer model agrees remarkably well with the six oil slick samples, correctly describing the pattern of mass removal in the GC×GC chromatogram as well as the progression of hydrocarbon removal with increasing sample age. A more quantitative analysis of the observed and simulated removal patterns is reported in the next section.

These measurement and modeling results imply fast evaporation and dissolution rates of oil hydrocarbons, when compared to other field studies. >50% losses of n-alkanes up to n-C_{12} within 4.1[25] to 6 h[17] have been reported in two oil spill field experiments during which ≤2 m^3 of oil was spilt. Ezra et al.[105] reported removal of volatile compounds up to n-C_{15} after 3 weeks for a beached residual fuel oil on the southeastern Mediterranean coast. Similarly, based on mass transfer calculations and field measurements at Nyes Neck beach, MA, Arey et al.[43] proposed a half-life of about 1 week for n-C_{15} in a ∼0.04 mm thick coating of heavy fuel oil on beach cobbles. Early weathering rates at those field sites were also comparable to early weathering observed in Prince William Sound after the 1989 *Exxon Valdez* spill.[3] Compared to these previous field studies, our oil slick samples exhibited relatively fast losses of light (≤n-C_{17}) hydrocarbons.

Oil sheen samples exhibited yet faster fractionation rates than oil slick samples. We observed >50% losses for compounds more volatile than n-C_{17} after only 1 h and up to n-C_{19} after 4 h. GC×GC chromatograms of oil sheen samples show dramatically accelerated removal of resolved and unresolved hydrocarbon mass, when compared to oil slick samples of the same age (Figures 1, S-8). Colloidal structures, which include films, water-in-oil emulsions, and dispersions,[106] play a major role in determining oil fractionation rate.[4,9,107−109] A very thin oil layer can fractionate very quickly: for example, while investigating ascending oil droplets from Santa Barbara natural offshore oil seep, Wardlaw and co-workers[9] estimated that a thin oil film of 0.3 μm thickness on the sea would exhibit significant evaporative losses of compounds in the C_{12}−C_{15} volatility range within minutes. Similarly, samples taken in 2012 from sheens appearing at the sea surface above the site of the *Deepwater Horizon* disaster were depleted of compounds more volatile than n-C_{15}.[110] We did not attempt to make meaningful comparisons between the mass transfer model results and oil sheen samples, since the model was parametrized for the oil slick. Sheen samples have unknown histories and were assumed to have departed from or remixed with slick material at unknown times.

GC×GC−FID brings several important advantages to the present field study, complementing the GC−FID and GC−MS techniques conventionally employed for analysis of oil mixtures in the environment. GC×GC retention time information enables the estimation of environmental partitioning properties of all resolved and unresolved hydrocarbon material in the n-C_9 to n-C_{25} elution range.[72,111] By comparison, conventional GC retention times do not enable estimates of environmental partitioning properties other than vapor pressure and boiling point, and thus they convey limited information about the environmental fate of the unresolved hydrocarbon mass. Additionally, the FID instrument response factor can be assumed similar (±12%) for different analyzed hydrocarbon compounds.[77−79] Thus, it is possible to measure and also model the quantitative mass changes in the complete resolved and unresolved GC×GC-amenable hydrocarbon material that arises in different samples. By comparison, the 52 individual compounds that we quantified by GC−FID and GC−MS in the neat oil account for only 1.6% of the mass of this particular crude oil (SI Table S-3). The GC−FID chromatogram of this oil presents a prominent unresolved complex mixture, likely arising from biodegradation in the Grane crude oil field that is characterized by at least two phases of oil reservoir charge.[112]

Diagnosing Evaporation and Dissolution of Hydrocarbons Using Mass Loss Tables (MLTs). To differentiate signatures of evaporation and dissolution in a quantitative way, we converted GC×GC chromatogram data into mass loss tables (MLTs).[44] MLTs are generated from finite element cells delineated by contours of estimated hydrocarbon vapor pressure and estimated aqueous solubility overlaid onto the GC×GC retention time space[44] (Figure 1b). MLTs show the mass losses of individual cells in a weathered sample relative to the neat oil, organized in volatility-vs-aqueous solubility space

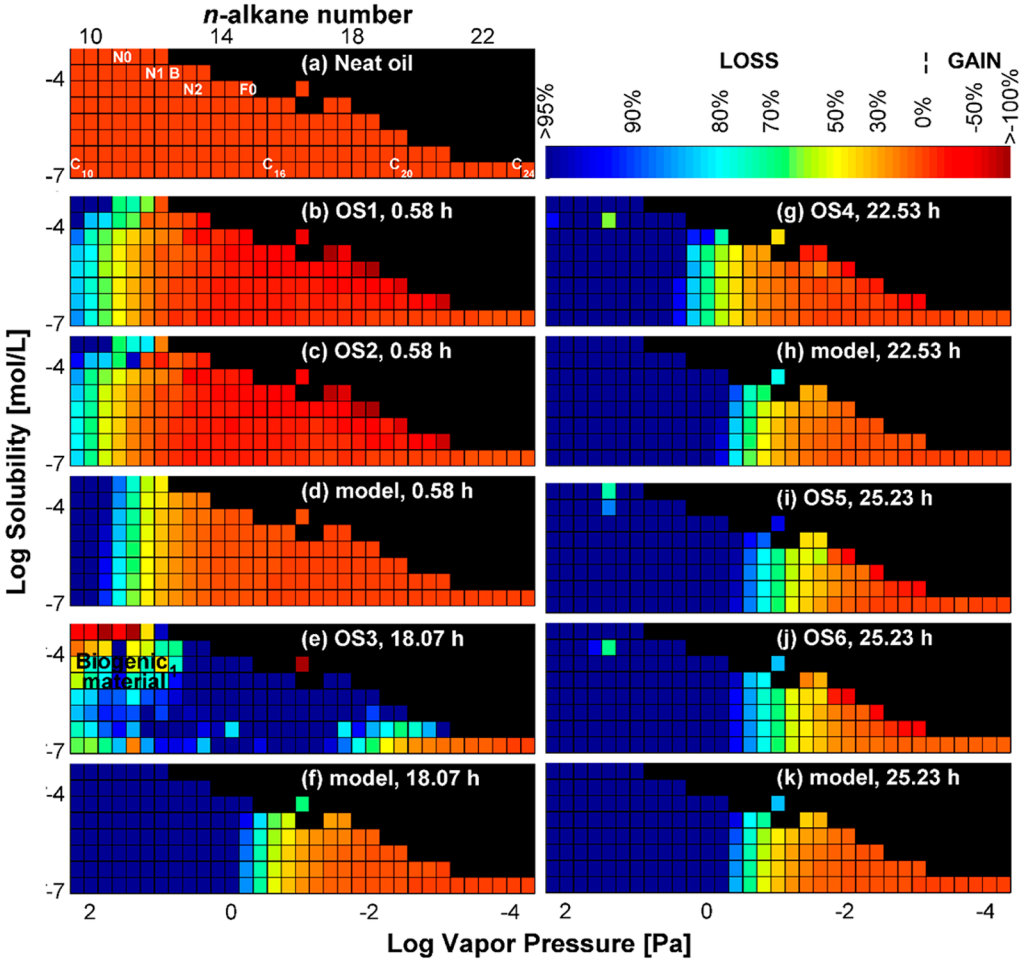

Figure 2. Mass loss tables (MLTs) showing fractionation of petroleum hydrocarbon mass removed from oil slick samples, organized as cells of compound groups in volatility versus solubility space. The color bar indicates the percentage of mass lost from a sample cell relative to the neat oil reference; negative values represent mass gains. Positions of the cells on the neat oil chromatogram are given in Figure 1b. Black cells correspond to property values not explored by compounds in the oil mixture or to cells containing mostly noise, defined as those containing less than 0.02% of the total signal contained in the part of the chromatogram covered by the MLTs, for neat oil. (a) The neat oil reference with labeled positions of selected compounds in the MLT space (refer to Figure 1 for abbreviations); (b-k) modeled MLTs and observed sample MLTs for oil slick samples OS1 to OS6. The time after the end of the oil release is indicated for each MLT. [1] Signal arising in the upper left region of the MLT for sample OS3 is thought to be biogenic material arising from the seawater incidentally included in this sample.

(Figure 2). This allows a straightforward visualization of the dominant physical processes leading to fractionation of the oil slick samples: aqueous dissolution leads to disappearance of hydrocarbon mass progressively from top rows to bottom rows of the MLT, whereas evaporation removes mass from leftmost columns progressively toward columns on the right. The MLTs also provide a basis for quantitative comparisons between mass transfer model predictions and observed fractionation patterns in oil slick samples from the field.

In agreement with the mass transfer model predictions, MLTs of collected oil slick samples exhibited an evaporation front progressing through time according to a decelerating trend (Figures 2 and S-9). Evaporation is the dominant fractionation process, based on inspection of the MLTs. With the exception of sample OS3, the position of the evaporation front predicted by the model agrees with collected oil slick samples to within 1 log vapor pressure unit (SI Figure S-9). Overall, the root-mean-squared-deviation (rmsd) of model-predicted MLTs with respect to sample MLTs was 0.38 in the log $M_i(t)/M_i(t_0)$ over the 155 MLT cells considered in each of the six oil slick field samples, thus entailing a comparison of model versus observations for 930 cells in total. This implies, for example, that if 80% mass loss was observed for a particular MLT cell, the model typically predicted a mass loss ranging from 52 to 92% for this cell. We interpret that the model captured the dominant evaporative weathering trend correctly (Figure 2).

Subtle dissolution signatures are also evident in the MLT data of several oil slick samples, distinct from evaporation trends. Samples OS1 and OS2, taken 0.58 h after the end of the oil release, both show signs of dissolution. For both of these samples, the uppermost rows of the MLT exhibit mass removal that is superimposed onto the evaporation signature (Figure 2). Samples OS4 and OS5, taken at 22.53 and 25.23 h, also exhibit a possible dissolution signature. By comparison, mass transfer simulations appear to underpredict dissolution extent at 0.58 h but are in closer agreement with compositional data for samples taken >20 h after the release.

Our analysis of hydrocarbon evaporation and dissolution processes takes a fundamental departure from conventional techniques that focus on the environmental behaviors of selected individual hydrocarbons that constitute a small fraction

dx.doi.org/10.1021/es502437e | Environ. Sci. Technol. 2014, 48, 9400−9411

of the oil. Here, we compare model simulations and field observations of mass transfer fractionations affecting all resolved and unresolved hydrocarbon material in the 174 to 391 °C boiling point range. This elution window contains 44% of the total oil mass and it comprises most of the hydrocarbon components that are affected by mass transfer during the initial 24 h after an oil release in the environment. Some other approaches model evaporation using pseudocomponents based on oil distillation curves;[63,71] however, this cannot capture the dissolution process.

Hydrocarbon Contamination of the Water Column at 1.5 m Depth. Four water column samples taken at 1.5 m depth from three sampling locations, 20 h after the oil release, were analyzed for several individual hydrocarbon compounds (SI Table S-3). For nine compounds having measured sample concentration values that exceeded the field blank value, we found that water column levels of extractable hydrocarbons implied mass apportionments to the water column that far exceeded the total hydrocarbon mass released during the spill (SI Table S-6). Our confounded results may plausibly have arisen from cross-contamination of water column samples from the oil slick during sampling; other analytical error; field sampling variability; contamination from boats used during the experiment; or high background levels of hydrocarbons arising from resuspension of sediments due to the convective mixing regime of the water column. We thus concluded that the water column data were unreliable, and we omit further consideration of these results from the study.

Simulated Hydrocarbon Mass Apportionments to Air and Water. The mass transfer model allows the simulation of time-dependent apportionments of hydrocarbon mass transferred to air and water (SI Figure S-10). According to the model, 74.0% of the whole oil remained in the slick, 25.7% was evaporated, and 0.3% was dissolved, 25 h after the oil release. Predictions after 2 days (71.1%, 28.4%, and 0.5% respectively) suggest that mass transfer rates decelerated rapidly after the first day (see also SI Animation S-1). Dispersion was estimated to be 0.7% based on the ADIOS model, 25 h after the oil release; this process was not considered in our mass transfer model.

Compound-specific mass apportionments were also calculated. Simulations predicted that 10% of naphthalene became dissolved and 90% was evaporated during the course of the experiment. According to the model, naphthalene was predicted to be already 52% depleted from the oil slick at the end of the oil release period, and 99% depleted 1 h later. Compound-specific mass apportionment predictions for BTEX, naphthalene, phenanthrene, anthracene, and n-C_7 to n-C_{18} n-alkanes are shown in Table S-7. BTEX compounds were predicted to disappear very rapidly from the oil slick. Benzene became 13% dissolved and 87% evaporated, whereas toluene was 5% dissolved and 95% evaporated, according to our model.

Studying a thicker slick of emulsified Grane crude oil in ice-cold seawater, others have observed slower evaporation rates, reporting 10−18% evaporative mass loss after 2 days.[11] Compared to our experiment, decelerated evaporation rate would be expected under colder temperatures, increased oil slick thickness, and water-in-oil emulsification. For example, our model would predict ∼17% evaporative mass loss if our experiment had taken place at 0 °C (Figure S-11). For comparison, Wolfe et al. estimated that ∼10% of *Exxon Valdez* oil mass had evaporated within 1−2 days and that 3.5% was dispersed into the water column within the first 3 days of the 1989 oil spill in Prince William Sound, Alaska.[3] At these different sites, the mass transfer rates to air and water were dependent on oil composition, ambient temperature, turbulence-induced emulsification, and other environmental conditions.

Hydrocarbon Evaporation Predicted by the Expressions of Fingas and by the ADIOS Model. We briefly evaluated the evaporation extent predicted by two empirical equations developed by Fingas[113] and also by the ADIOS oil spill model[63] (SI Section S-9). Both models underestimated early evaporation rates for the end of the present experiment. The Fingas equations predict an evaporation extent that would be equivalent to the loss of hydrocarbons up to only n-C_{10} after 25.23 h, assuming that volatilization progressively removes hydrocarbons from the oil according to decreasing boiling point (Figure 1j). By similar reasoning, the ADIOS model would predict evaporative removal up to n-C_{13} (SI Section S-9). By comparison, the mass transfer model of the present study predicted >50% evaporative removal up to n-C_{16} after 25.23 h, in closer agreement with collected oil slick samples that exhibited >50% removal up to n-C_{17} (Figure 1j, SI Table S-5). Oil slick thickness is not considered in the Fingas equations; however, the thickness plays an influential role in mass transfer rate of hydrocarbons during an oil spill.[4,43,53,61] The thickness of an oil slick of a given volume is expected to influence the total mass loss rate by evaporation. This arises from the physics of interfaces, where the rate of mass loss depends on area of the interface (SI Section S-6). This interpretation is supported by reports from other field studies,[9,110] as well as by the fact that collected oil sheens exhibited accelerated evaporative losses compared to thicker oil slick samples during our experiment (Figures 1, 2, S-8, S-12). Nonetheless oil slick thickness is not included in some models used to describe mass loss rates from oil.[114]

Implications for Early Mass Transfer Processes and Resulting Ecological Exposures During Oil Spills. To our knowledge, this is the first study to report on the broad-spectrum compositional evolution of an oil slick undergoing simultaneous evaporation and dissolution during the initial day of an open sea oil spill. Early fluxes of evaporated hydrocarbons are relevant for anticipating the inhalation exposure levels of downwind populations or personnel involved in emergency response.[115] Dissolution and dispersion of hydrocarbons into the water column control the exposures of marine organisms, and these exposures may be the most elevated during the initial hours or days after a release. However, for many light hydrocarbons, the kinetics of evaporation compete directly with kinetics of dissolution, and these two processes are thus difficult to disentangle in the field.

Ambient environmental conditions regulated the oil slick behavior and early mass transfer processes during this oil spill. With the aid of the mass transfer model, we can infer outcomes that may be expected under other temperature conditions, wind conditions, and water column stability conditions, and these are each discussed in turn below.

Evaporation flux and dissolution flux are both expected to be decelerated at low temperatures compared to higher temperatures. However, vapor pressure decreases with decreasing temperature more steeply than does aqueous solubility, for hydrocarbons.[81] Additionally, with decreasing temperature, diffusion coefficients in air and water both decrease, leading to decreased mass transfer velocities (length time^{-1}) through the air and water boundary layers. Among these competing temperature effects, the temperature dependence of vapor

pressure is expected to dominate. Thus, cold weather conditions are expected to produce increased mass apportionments to water relative to air, for the compounds that we studied. For example, according to the mass transfer model, a spill of Grane crude oil in cold seawater (3 °C) would experience dissolution extent increased by 60% and evaporation extent decreased by 40% compared to the same spill in warm seawater (33 °C) (Figure S-11). In interpreting these predictions, the reader should bear in mind that our model includes a temperature correction to vapor pressure but not to aqueous solubility. The solubility correction may be significant for PAHs: aqueous solubility is decreased by 40% for naphthalene and 86% for phenanthrene at 3 °C compared to 33 °C.[81] This is discussed further in SI Section S-16.

Wind speed strongly influences early mass transfer rates of hydrocarbons. Air and water boundary layer thicknesses are both decreased by increasing wind speed, and therefore increasing wind speed will lead to increased mass transfer rates to both air and water (SI Figure S-13). Additionally, the entrainment of oil droplets into the water column would become important at wind speeds higher than those encountered during the experiment.[63,103] Thus, under higher wind speed conditions, substantially higher quantities of hydrocarbons would become dispersed and would thereby lead to increased dissolution.

For this field experiment, the modeled vertical turbulent mixing coefficient, *E*, had little impact on total mass of hydrocarbons dissolved into the water column. However, *E* largely dictates the volume of water into which the hydrocarbons are diluted and thus the depth to which marine organisms are exposed. Our experiment took place in a shallow shelf sea during autumnal convection. This led to a high vertical turbulent mixing coefficient and no water column stratification, with dissolved hydrocarbons predicted to reach the sea bottom (42 m depth) within hours. For a stratified water column, the turbulent mixing coefficient near the sea surface usually will depend on the wind speed. Water column stability is also relevant to deep sea oil releases. For example, during the *Deepwater Horizon* oil spill, ∼1100 m depth intrusions of dissolved hydrocarbons into the highly stable Gulf of Mexico water column exhibited narrow vertical variability as far as 10 km downstream from the emission point.[7]

The thickness of the oil layer affects the fractionation rates of highly toxic and soluble compounds such as naphthalene or phenanthrene. For example, the very rapid hydrocarbon fractionation exhibited by sheen samples, relative to slick samples, is related to the oil sheen thickness, which was estimated to lie near 0.1−0.3 μm according to its color.[116] By comparison, the oil slick thickness was an estimated 10 μm after the first hour of the experiment and decreased to an estimated thickness of <1 μm by the end of the experiment (Figure S-14). A thinner slick would lead to more rapid fractionation of oil hydrocarbons arising from evaporation and dissolution. However, beneath a larger and thicker slick, higher concentrations within the water column would be expected, due to the larger load of oil mass per area of sea surface (calculations not shown).

Finally, the present study points to a key area where further insight is needed. Reliable water column composition data would prove an invaluable complement to oil slick composition data during the very early stages of an oil spill. This would provide a basis for closing the mass balance on estimated mass transfers to the water column. This includes the evaluation of accelerated hydrocarbon mass transfer rates resulting from entrainment of whole oil droplets in the water column,[108] addition of dispersants,[117] and DOC-enhanced mass transfer of hydrocarbons to the aqueous phase.[118] Additionally, under more energetic sea surface conditions than those reported here, early hydrocarbon mass transfers to the water column may be more difficult to estimate, due to turbulent entrainment of oil into the water column. A better understanding of these mechanisms and additional early field sample data are needed in order to properly assess ecological exposures during the initial hours and days of an oil spill.

■ ASSOCIATED CONTENT

Supporting Information

Grane crude oil properties and distillation data; field sampling procedures; wind speed and oil slick area observations; measured concentrations of individual compounds in water column and neat oil by GC−MS and GC−FID; instrument analysis methods; derivation of the mass transfer equations and comparison to other models; determination of the vertical turbulent mixing coefficient; partition property estimation from GC×GC retention data; comparison of our model with the Fingas and ADIOS models; measured mass losses of individual compounds in oil slick and oil sheen samples based on GC×GC−FID data; GC×GC−FID chromatograms of oil sheen samples; modeled and observed position of the evaporation front for oil slick samples; comparison of measured and model-predicted hydrocarbon concentrations in the water column; modeled mass apportionments of individual and total hydrocarbons to air and water; effects of temperature and wind speed on hydrocarbon mass apportionments to air and water; MLTs for oil sheen samples; and the modeled evolution of oil slick thickness. An animation (.avi file) of the simulated evolution of the GC×GC chromatogram, showing the modeled apportionments to atmosphere, water, and oil slick for GC×GC-amenable hydrocarbons, throughout the duration of the experiment. This material is available free of charge via the Internet at http://pubs.acs.org.

■ AUTHOR INFORMATION

Corresponding Author

*Phone: +41 21 693 80 31. E-mail: samuel.arey@epfl.ch.

Author Contributions

●These authors contributed equally.

Funding

This research was supported by grants from the NSF (OCE-0960841 and EAR-0950600), the BP/the Gulf of Mexico Research Initiative (GoMRI-015), the DEEP-C consortium, and the European Framework programs *FACEiT* (FP6, contract 018391) and *BACSIN* (FP7, contract KBBE-211684). It contributes to the 'Chemicals in the Environment' (CITE) research program of the Helmholtz Association.

Notes

The authors declare no competing financial interest.

■ ACKNOWLEDGMENTS

We thank Karin L. Lemkau (UCSB), Rob Modini (EPFL), Damien Bouffard (EPFL), Alfred Johny Wüest (EPFL), Oliver C. Mullins (Schlumberger), and Per Daling (SINTEF) for conversations about data interpretation and modeling. We gratefully acknowledge Louis Peperzak (NIOZ) and the crew of the *Arca* for field logistics. We also thank Rebecca Rutler for

assistance with sample analysis and Flavio Comino for construction of the water column grab sampler.

REFERENCES

(1) *Oil in the Sea III: Inputs, Fates, and Effects*; The National Academies Press: Washington, DC, 2003.
(2) Mackay, D.; Shiu, W. Y. Aqueous solubilities of weathered northern crude oils. *Bull. Environ. Contam. Toxicol.* **1976**, *15*, 101−109.
(3) Wolfe, D. A.; Hameedi, M. J.; Galt, J. A.; Watabayashi, G.; Short, J.; O'Claire, C.; Rice, S.; Michel, J.; Payne, J. R.; Braddock, J.; Hanna, S.; Sale, D. The fate of the oil spilled from the *Exxon Valdez*. *Environ. Sci. Technol.* **1994**, *28*, 560A−568A.
(4) Harrison, W.; Winnik, M. A.; Kwong, P. T. Y.; Mackay, D. Disappearance of aromatic and aliphatic components from small sea surface slicks. *Environ. Sci. Technol.* **1975**, *9*, 231−234.
(5) *Proceedings of a symposium on preliminary results from the September 1979 Researcher/Pierce Ixtoc-1 cruise*; National Oceanic and Atmospheric Administration, Office of Marine Pollution Assessment: Boulder, USA, 1980.
(6) Boehm, P. D.; Cook, L. L.; Murray, K. J. Aromatic hydrocarbon concentrations in seawater: *Deepwater Horizon* oil spill. *Int. Oil Spill Conf. Proc.* **2011**, *2011*, abs371.
(7) Reddy, C. M.; Arey, J. S.; Seewald, J. S.; Sylva, S. P.; Lemkau, K. L.; Nelson, R. K.; Carmichael, C. A.; McIntyre, C. P.; Fenwick, J.; Ventura, G. T.; Mooy, B. A. S. V.; Camilli, R. Composition and fate of gas and oil released to the water column during the *Deepwater Horizon* oil spill. *Proc. Natl. Acad. Sci. U. S. A.* **2012**, *109*, 20229−20234.
(8) Ryerson, T. B.; Aikin, K. C.; Angevine, W. M.; Atlas, E. L.; Blake, D. R.; Brock, C. A.; Fehsenfeld, F. C.; Gao, R.-S.; de Gouw, J. A.; Fahey, D. W.; Holloway, J. S.; Lack, D. A.; Lueb, R. A.; Meinardi, S.; Middlebrook, A. M.; Murphy, D. M.; Neuman, J. A.; Nowak, J. B.; Parrish, D. D.; Peischl, J.; Perring, A. E.; Pollack, I. B.; Ravishankara, A. R.; Roberts, J. M.; Schwarz, J. P.; Spackman, J. R.; Stark, H.; Warneke, C.; Watts, L. A. Atmospheric emissions from the *Deepwater Horizon* spill constrain air-water partitioning, hydrocarbon fate, and leak rate. *Geophys. Res. Lett.* **2011**, *38*, L07803.
(9) Wardlaw, G. D.; Arey, J. S.; Reddy, C. M.; Nelson, R. K.; Ventura, G. T.; Valentine, D. L. Disentangling oil weathering at a marine seep using GC×GC: Broad metabolic specificity accompanies subsurface petroleum biodegradation. *Environ. Sci. Technol.* **2008**, *42*, 7166−7173.
(10) Ross, S.; Potter, S.; Belore, R.; Lewis, A. Dispersant testing at Ohmsett: Feasibility study and preliminary testing. *Int. Oil Spill Conf. Proc.* **2001**, 461−466.
(11) *Meso-scale weathering of oil as a function of ice conditions. Oil properties, dispersability and in-situ burnability of weathered oil as a function of time*; JIP Report; 19; SINTEF Materials and Chemistry, Marine Environmental Technology: 2010.
(12) Barth, T. Weathering of crude oil in natural marine environments: The concentration of polar degradation products in water under oil as measured in several field studies. *Chemosphere* **1984**, *13*, 67−86.
(13) Genders, S. In-situ detection and tracking of oil in the water column. *Oil Chem. Pollut.* **1988**, *4*, 113−126.
(14) Johansen, Ø.; Rye, H.; Cooper, C. DeepSpill−Field study of a simulated oil and gas blowout in deep water. *Spill Sci. Technol. Bull.* **2003**, *8*, 433−443.
(15) Daling, P. S.; Strøm, T. Weathering of oils at sea: Model/field data comparisons. *Spill Sci. Technol. Bull.* **1999**, *5*, 63−74.
(16) Daling, P. S.; Singsaas, I.; Reed, M.; Hansen, O. Experiences in dispersant treatment of experimental oil spills. *Spill Sci. Technol. Bull.* **2002**, *7*, 201−213.
(17) Smith, C. L.; MacIntyre, W. G. Initial aging of fuel oil films of sea water. *Int. Oil Spill Conf. Proc.* **1971**, 457−461.
(18) Brussaard, C. P. D.; Peperzak, L.; Witte, Y.; Huisman, J. An experimental oil spill at sea. In *Handbook of Hydrocarbon and Lipid Microbiology*; Timmis, K. N., Ed.; Springer: Berlin Heidelberg, 2010; pp 3491−3502.
(19) Cormack, D.; Nichols, J. A. The concentrations of oil in sea water resulting from natural and chemically induced dispersion of oil slicks. *Int. Oil Spill Conf. Proc.* **1977**, 381−385.
(20) Jeffery, P. G. Large-scale experiments on the spreading of oil at sea and its disappearance by natural factors. *Int. Oil Spill Conf. Proc.* **1973**, 469−474.
(21) Gill, S. D. Dispersant field trials in Canadian waters. *Int. Oil Spill Conf. Proc.* **1977**, 391−394.
(22) Fingas, M.; Brown, C. E. Oil spill remote sensing: A forensic approach. In *Oil Spill Environmental Forensics*; Wang, Z., Stout, S. A., Eds.; Academic Press: Burlington, 2007; pp 419−447.
(23) Sivadier, H. O.; Mikolaj, P. G. Measurement of evaporation rates from oil slicks on the open sea. *Int. Oil Spill Conf. Proc.* **1973**, 475−484.
(24) Lichtenthaler, R. G.; Daling, P. S. Dispersion of chemically treated crude oil in Norwegian offshore waters. *Int. Oil Spill Conf. Proc.* **1983**, 7−14.
(25) Delvigne, G. A. L. Experiments on natural and chemical dispersion of oil in laboratory and field circumstances. *Int. Oil Spill Conf. Proc.* **1985**, 507−514.
(26) Gill, S. D.; Goodman, R. H.; Swiss, J. Halifax '83 sea trial of oil spill dispersant concentrates. *Int. Oil Spill Conf. Proc.* **1985**, 479−482.
(27) Lange, R. A 100 tons experimental oil spill at Halten Bank, off Norway. *Int. Oil Spill Conf. Proc.* **1985**, 503−505.
(28) Buist, I. A.; Dickins, D. F. Experimental spills of crude oil in pack ice. *Int. Oil Spill Conf. Proc.* **1987**, 373−381.
(29) McAuliffe, C. D. The weathering of volatile hydrocarbons from crude oil slicks on water. *Int. Oil Spill Conf. Proc.* **1989**, 357−363.
(30) Hurford, N.; Buchanan, I. Results of the 1987 forties crude oil trial in the North Sea. *Int. Oil Spill Conf. Proc.* **1989**, 525−532.
(31) Reed, M.; Turner, C.; Price, J. Implications of observations of intentional oil spills. *Int. Oil Spill Conf. Proc.* **1993**, 617−622.
(32) Lunel, T. Dispersant effectiveness at sea. *Int. Oil Spill Conf. Proc.* **1995**, 147−155.
(33) Rye, H.; Brandvik, P. J. Verification of subsurface oil spill models. *Int. Oil Spill Conf. Proc.* **1997**, 551−557.
(34) Belore, R. C.; Trudel, B. K.; Lee, K. Correlating wave tank dispersant effectiveness tests with at-sea trials. *Int. Oil Spill Conf. Proc.* **2005**, 65−70.
(35) Brekne, T. M.; Eide, G. A.; Skeie, G. M. Full scale implementation of state-of-the-art mechanical oil spill response technology on the Norwegian continental shelf. *Int. Oil Spill Conf. Proc.* **2005**, 831−836.
(36) Dickins, D.; Brandvik, P. J.; Bradford, J.; Faksness, L.-G.; Liberty, L.; Daniloff, R. Svalbard 2006 experimental oil spill under ice: Remote sensing, oil weathering under Arctic conditions and assessment of oil removal by in-situ burning. *Int. Oil Spill Conf. Proc.* **2008**, 681−688.
(37) Lewis, A.; Daling, P. S.; Strøm-Kristiansen, T.; Nordvik, A. B.; Fiocco, R. J. Weathering and chemical dispersion of oil at sea. *Int. Oil Spill Conf. Proc.* **1995**, 157−164.
(38) Daling, P. S.; Aamo, O. M.; Lewis, A.; Strøm-Kristiansen, T. SINTEF/IKU oil-weathering model: Predicting oils' properties at sea. *Int. Oil Spill Conf. Proc.* **1997**, 297−307.
(39) Stout, S. A.; Wang, Z. Chemical fingerprinting of spilled or discharged petroleum — methods and factors affecting petroleum fingerprints in the environment. In *Oil Spill Environmental Forensics*; Wang, Z.; Stout, S. A., Eds.; Academic Press: Burlington, 2007; pp 1−53.
(40) Fingas, M. F. Studies on the evaporation of crude oil and petroleum products: I. The relationship between evaporation rate and time. *J. Hazard. Mater.* **1997**, *56*, 227−236.
(41) Short, J. W.; Irvine, G. V.; Mann, D. H.; Maselko, J. M.; Pella, J. J.; Lindeberg, M. R.; Payne, J. R.; Driskell, W. B.; Rice, S. D. Slightly weathered *Exxon Valdez* oil persists in Gulf of Alaska beach sediments after 16 years. *Environ. Sci. Technol.* **2007**, *41*, 1245−1250.
(42) Irvine, G. V.; Mann, D. H.; Short, J. W. Multi-year persistence of oil mousse on high energy beaches distant from the *Exxon Valdez* spill origin. *Mar. Pollut. Bull.* **1999**, *38*, 572−584.

(43) Arey, J. S.; Nelson, R. K.; Plata, D. L.; Reddy, C. M. Disentangling oil weathering using GC×GC. 2. Mass transfer calculations. *Environ. Sci. Technol.* **2007**, *41*, 5747−5755.
(44) Arey, J. S.; Nelson, R. K.; Reddy, C. M. Disentangling oil weathering using GC×GC. 1. Chromatogram analysis. *Environ. Sci. Technol.* **2007**, *41*, 5738−5746.
(45) Riazi, M. R.; Edalat, M. Prediction of the rate of oil removal from seawater by evaporation and dissolution. *J. Pet. Sci. Eng.* **1996**, *16*, 291−300.
(46) Incardona, J. P.; Vines, C. A.; Anulacion, B. F.; Baldwin, D. H.; Day, H. L.; French, B. L.; Labenia, J. S.; Linbo, T. L.; Myers, M. S.; Olson, O. P.; Sloan, C. A.; Sol, S.; Griffin, F. J.; Menard, K.; Morgan, S. G.; West, J. E.; Collier, T. K.; Ylitalo, G. M.; Cherr, G. N.; Scholz, N. L. Unexpectedly high mortality in Pacific herring embryos exposed to the 2007 *Cosco Busan* oil spill in San Francisco Bay. *Proc. Natl. Acad. Sci. U. S. A.* **2011**, 201108884.
(47) Incardona, J. P.; Vines, C. A.; Linbo, T. L.; Myers, M. S.; Sloan, C. A.; Anulacion, B. F.; Boyd, D.; Collier, T. K.; Morgan, S.; Cherr, G. N.; Scholz, N. L. Potent phototoxicity of marine bunker oil to translucent herring embryos after prolonged weathering. *PLoS One* **2012**, *7*, e30116.
(48) Rowland, S.; Donkin, P.; Smith, E.; Wraige, E. Aromatic hydrocarbon "humps" in the marine environment: Unrecognized toxins? *Environ. Sci. Technol.* **2001**, *35*, 2640−2644.
(49) Neff, J. M.; Ostazeski, S.; Gardiner, W.; Stejskal, I. Effects of weathering on the toxicity of three offshore Australian crude oils and a diesel fuel to marine animals. *Environ. Toxicol. Chem.* **2000**, *19*, 1809−1821.
(50) Reddy, C. M.; Quinn, J. G. The *North Cape* oil spill: Hydrocarbons in Rhode Island coastal waters and Point Judith Pond. *Mar. Environ. Res.* **2001**, *52*, 445−461.
(51) Boehm, P. D.; Neff, J. M.; Page, D. S. Assessment of polycyclic aromatic hydrocarbon exposure in the waters of Prince William Sound after the *Exxon Valdez* oil spill: 1989−2005. *Mar. Pollut. Bull.* **2007**, *54*, 339−356.
(52) Ryerson, T. B.; Camilli, R.; Kessler, J. D.; Kujawinski, E. B.; Reddy, C. M.; Valentine, D. L.; Atlas, E.; Blake, D. R.; de Gouw, J.; Meinardi, S.; Parrish, D. D.; Peischl, J.; Seewald, J. S.; Warneke, C. Chemical data quantify Deepwater Horizon hydrocarbon flow rate and environmental distribution. *Proc. Natl. Acad. Sci. U. S. A.* **2012**, 201110564.
(53) Lemkau, K. L. Comprehensive study of a heavy fuel oil spill: Modeling and analytical approaches to understanding environmental weathering, Ph.D. Dissertation, Massachusetts Institute of Technology and Woods Hole Oceanographic Institution: MA, USA, 2012.
(54) Chao, X.; Shankar, N. J.; Cheong, H. F. Two- and three-dimensional oil spill model for coastal waters. *Ocean Eng.* **2001**, *28*, 1557−1573.
(55) Guo, W. J.; Wang, Y. X. A numerical oil spill model based on a hybrid method. *Mar. Pollut. Bull.* **2009**, *58*, 726−734.
(56) Wang, J.; Shen, Y. Modeling oil spills transportation in seas based on unstructured grid, finite-volume, wave-ocean model. *Ocean Model.* **2010**, *35*, 332−344.
(57) Short, J. W.; Heintz, R. A. Identification of *Exxon Valdez* oil in sediments and tissues from Prince William Sound and the Northwestern Gulf of Alaska based on a PAH weathering model. *Environ. Sci. Technol.* **1997**, *31*, 2375−2384.
(58) Stiver, W.; Shiu, W. Y.; Mackay, D. Evaporation times and rates of specific hydrocarbons in oil spills. *Environ. Sci. Technol.* **1989**, *23*, 101−105.
(59) Drivas, P. J. Calculation of evaporative emissions from multicomponent liquid spills. *Environ. Sci. Technol.* **1982**, *16*, 726−728.
(60) Page, C. A.; Bonner, J. S.; Sumner, P. L.; Autenrieth, R. L. Solubility of petroleum hydrocarbons in oil/water systems. *Mar. Chem.* **2000**, *70*, 79−87.
(61) Luk, G. K.; Kuan, H. F. Modelling the behaviour of oil spills in natural waters. *Can. J. Civ. Eng.* **1993**, *20*, 210−219.
(62) French McCay, D. P.; Payne, J. R. Model of oil fate and water concentrations with and without application of dispersants. *Proc. 24th Arct. Mar. Oilspill Technol. Semin.* **2001**, 611−645.
(63) Lehr, W.; Jones, R.; Evans, M.; Simecek-Beatty, D.; Overstreet, R. Revisions of the ADIOS oil spill model. *Environ. Model. Softw.* **2002**, *17*, 189−197.
(64) Leinonen, P. J. The fate of spilled oil, Ph.D. Dissertation, University of Toronto: Toronto, 1976.
(65) Hibbs, D. E.; Gulliver, J. S. Dissolution rate coefficients for surface slicks on rivers. *Water Res.* **1999**, *33*, 1811−1816.
(66) Southworth, G. R.; Herbes, S. E.; Allen, C. P. Evaluating a mass transfer model for the dissolution of organics from oil films into water. *Water Res.* **1983**, *17*, 1647−1651.
(67) Mackay, D.; Leinonen, P. J. *Mathematical model of the behaviour of oil spills on water with natural and chemical dispersion*; EPS-3-EC-77-19; Department of Fisheries and the Environment: 1977.
(68) Yang, W. C.; Wang, H. Modeling of oil evaporation in aqueous environment. *Water Res.* **1977**, *11*, 879−887.
(69) Rye, H. A multicomponent oil spill model for dissolved aromatic concentrations. *Int. Oil Spill Conf. Proc.* **1995**, 49−53.
(70) Fingas, M. Chapter 3 - Introduction to oil chemistry and properties. In *Oil Spill Science and Technology*; Fingas, M., Ed.; Gulf Professional Publishing: Boston, 2011; pp 51−59.
(71) Reed, M.; Ekrol, N.; Daling, P.; Johansen, Ø.; Ditlevsen, M. K.; Swahn, I.; Myrhaug Resby, J. L.; Skognes, K. *SINTEF oil weathering model user's manual, Version 3.0*; SINTEF Materials and Chemistry: Trondheim, Norway, 2004.
(72) Arey, J. S.; Nelson, R. K.; Xu, L.; Reddy, C. M. Using comprehensive two-dimensional gas chromatography retention indices to estimate environmental partitioning properties for a complete set of diesel fuel hydrocarbons. *Anal. Chem.* **2005**, *77*, 7172−7182.
(73) *Crude oil assay, Grane*; Statoil: Norway, 2003; p 18.
(74) Gros, J.; Nabi, D.; Dimitriou-Christidis, P.; Rutler, R.; Arey, J. S. Robust algorithm for aligning two-dimensional chromatograms. *Anal. Chem.* **2012**, *84*, 9033−9040.
(75) Reichenbach, S. E.; Ni, M.; Zhang, D.; Ledford, E. B., Jr. Image background removal in comprehensive two-dimensional gas chromatography. *J. Chromatogr. A* **2003**, *985*, 47−56.
(76) Reichenbach, S. E.; Ni, M.; Kottapalli, V.; Visvanathan, A. Information technologies for comprehensive two-dimensional gas chromatography. *Chemom. Intell. Lab. Syst.* **2004**, *71*, 107−120.
(77) Gros, J.; Reddy, C. M.; Aeppli, C.; Nelson, R. K.; Carmichael, C. A.; Arey, J. S. Resolving biodegradation patterns of persistent saturated hydrocarbons in weathered oil samples from the *Deepwater Horizon* disaster. *Environ. Sci. Technol.* **2014**, *48*, 1628−1637.
(78) Tong, H. Y.; Karasek, F. W. Flame ionization detector response factors for compound classes in quantitative analysis of complex organic mixtures. *Anal. Chem.* **1984**, *56*, 2124−2128.
(79) Mullins, O. C.; Ventura, G. T.; Nelson, R. K.; Betancourt, S. S.; Raghuraman, B.; Reddy, C. M. Visible−near-infrared spectroscopy by downhole fluid analysis coupled with comprehensive two-dimensional gas chromatography to address oil reservoir complexity. *Energy Fuels* **2008**, *22*, 496−503.
(80) Eilers, P. H. C. Parametric time warping. *Anal. Chem.* **2004**, *76*, 404−411.
(81) Schwarzenbach, R. P.; Gschwend, P. M.; Imboden, D. M. *Environmental Organic Chemistry*, 2nd ed.; John Wiley & Sons: Hoboken, NJ, 2003.
(82) Fick, A. Ueber Diffusion. *Ann. Phys.* **1855**, *170*, 59−86.
(83) Einstein, A. Über die von der molekularkinetischen Theorie der Wärme geforderte Bewegung von in ruhenden Flüssigkeiten suspendierten Teilchen. *Ann. Phys.* **1905**, *322*, 549−560.
(84) Fischer, H. B.; List, E. J.; Koh, R. C. Y.; Imberger, J.; Brooks, N. H. *Mixing in Inland and Coastal Waters*; Academic Press: London, 1979.
(85) Brown, J. W.; Churchill, R. V. *Fourier Series and Boundary Value Problems*, 5th ed.; McGraw-Hill: New York, 1993.
(86) Becker, J. J.; Sandwell, D. T.; Smith, W. H. F.; Braud, J.; Binder, B.; Depner, J.; Fabre, D.; Factor, J.; Ingalls, S.; Kim, S.-H.; Ladner, R.;

Marks, K.; Nelson, S.; Pharaoh, A.; Trimmer, R.; Von Rosenberg, J.; Wallace, G.; Weatherall, P. Global bathymetry and elevation data at 30 arc seconds resolution: SRTM30_PLUS. *Mar. Geod.* **2009**, *32*, 355−371.
(87) Xie, H.; Yapa, P. D.; Nakata, K. Modeling emulsification after an oil spill in the sea. *J. Mar. Syst.* **2007**, *68*, 489−506.
(88) Xu, D.; Lu, H.; Yu, D. On the relationships between the mean wavelength and wave-period of wind waves in deep water. *Appl. Ocean Res.* **1999**, *21*, 127−131.
(89) Ichiye, T. Upper ocean boundary-layer flow determined by dye diffusion. *Phys. Fluids* **1967**, *10*, S270.
(90) Hu, H.; Wang, J. Modeling effects of tidal and wave mixing on circulation and thermohaline structures in the Bering Sea: Process studies. *J. Geophys. Res. Oceans* **2010**, *115*.
(91) Brutsaert, W. *Evaporation into the Atmosphere*; Kluwer Academic Publishers: Dordrecht, Netherlands, 1982.
(92) Ambaum, M. H. P. *Thermal Physics of the Atmosphere*; John Wiley & Sons: Chichester, UK, 2010.
(93) Kumar, L.; Andrew, K. S.; Knowles, E. Modelling topographic variation in solar radiation in a GIS environment. *Int. J. Geogr. Inf. Sci.* **1997**, *11*, 475−497.
(94) Becker, G. A. Beitrage zur Hydrographie und Wärmebilanz der Nordsee. *Dtsch. Hydrogr. Z.* **1981**, *34*, 167−262.
(95) Pohlmann, T. Calculating the annual cycle of the vertical eddy viscosity in the North Sea with a three-dimensional baroclinic shelf sea circulation model. *Cont. Shelf Res.* **1996**, *16*, 147−161.
(96) Wüest, A.; Carmack, E. A priori estimates of mixing and circulation in the hard-to-reach water body of Lake Vostok. *Ocean Model.* **2000**, *2*, 29−43.
(97) Mackay, D.; Shiu, W. Y.; Ma, K.-C.; Lee, S. C. *Handbook of Physical-Chemical Properties and Environmental Fate for Organic Chemicals*, 2nd ed.; Taylor & Francis: Boca Raton, Florida, U.S.A., 2006.
(98) Xie, W.-H.; Shiu, W.-Y.; Mackay, D. A review of the effect of salts on the solubility of organic compounds in seawater. *Mar. Environ. Res.* **1997**, *44*, 429−444.
(99) Tsonopoulos, C. Thermodynamic analysis of the mutual solubilities of normal alkanes and water. *Fluid Phase Equilib.* **1999**, *156*, 21−33.
(100) Ferguson, A. L.; Debenedetti, P. G.; Panagiotopoulos, A. Z. Solubility and molecular conformations of *n*-alkane chains in water. *J. Phys. Chem. B* **2009**, *113*, 6405−6414.
(101) McCain, W. D., Jr. *The Properties of Petroleum Fluids*; 2nd ed.; PennWell: Tulsa, 1990.
(102) Sebastião, P.; Guedes Soares, C. Modeling the fate of oil spills at sea. *Spill Sci. Technol. Bull.* **1995**, *2*, 121−131.
(103) Delvigne, G. A. L.; Sweeney, C. E. Natural dispersion of oil. *Oil Chem. Pollut.* **1988**, *4*, 281−310.
(104) Yapa, P. Modeling oil spills to mitigate coastal pollution. In *Handbook of Environmental Fluid Dynamics, Vol. two*; CRC Press: 2012; pp 243−256.
(105) Ezra, S.; Feinstein, S.; Pelly, I.; Bauman, D.; Miloslavsky, I. Weathering of fuel oil spill on the east Mediterranean coast, Ashdod, Israel. *Org. Geochem.* **2000**, *31*, 1733−1741.
(106) Hiemenz, P. C.; Rajagopalan, R. *Principles of Colloid and Surface Chemistry*, 3rd ed.; Marcel Dekker: New York, 1997.
(107) Irvine, G. V.; Mann, D. H.; Short, J. W. Persistence of 10-year old *Exxon Valdez* oil on Gulf of Alaska beaches: The importance of boulder-armoring. *Mar. Pollut. Bull.* **2006**, *52*, 1011−1022.
(108) Mackay, D.; Buist, I.; Mascarenhas, R.; Paterson, S. *Oil spill processes and models*; EE-8; Environment Canada, 1980.
(109) Thorpe, S. A. Langmuir circulation and the dispersion of oil spills in shallow seas. *Spill Sci. Technol. Bull.* **2000**, *6*, 213−223.
(110) Aeppli, C.; Reddy, C. M.; Nelson, R. K.; Kellermann, M. Y.; Valentine, D. L. Recurrent oil sheens at the *Deepwater Horizon* disaster site fingerprinted with synthetic hydrocarbon drilling fluids. *Environ. Sci. Technol.* **2013**, *47*, 8211−8219.
(111) Nabi, D.; Gros, J.; Dimitriou-Christidis, P.; Arey, J. S. Mapping environmental partitioning properties of nonpolar complex mixtures using GC×GC. *Environ. Sci. Technol.* **2014**, *48*, 6814−6826.
(112) Justwan, H.; Dahl, B.; Isaksen, G. H. Geochemical characterisation and genetic origin of oils and condensates in the South Viking Graben, Norway. *Mar. Pet. Geol.* **2006**, *23*, 213−239.
(113) Fingas, M. F. Modeling evaporation using models that are not boundary-layer regulated. *J. Hazard. Mater.* **2004**, *107*, 27−36.
(114) Fingas, M. Chapter 9 - Evaporation modeling. In *Oil Spill Science and Technology*; Fingas, M., Ed.; Gulf Professional Publishing: Boston, 2011; pp 201−242.
(115) Middlebrook, A. M.; Murphy, D. M.; Ahmadov, R.; Atlas, E. L.; Bahreini, R.; Blake, D. R.; Brioude, J.; de Gouw, J. A.; Fehsenfeld, F. C.; Frost, G. J.; Holloway, J. S.; Lack, D. A.; Langridge, J. M.; Lueb, R. A.; McKeen, S. A.; Meagher, J. F.; Meinardi, S.; Neuman, J. A.; Nowak, J. B.; Parrish, D. D.; Peischl, J.; Perring, A. E.; Pollack, I. B.; Roberts, J. M.; Ryerson, T. B.; Schwarz, J. P.; Spackman, J. R.; Warneke, C.; Ravishankara, A. R. Air quality implications of the *Deepwater Horizon* oil spill. *Proc. Natl. Acad. Sci. U. S. A.* **2012**, *109*, 20280−20285.
(116) *Aerial observations of oil at sea*; HAZMAT; 96-7; National Oceanic and Atmospheric Administration, Office of Ocean Resources Conservation and Assessment, Hazardous Materials Response and Assessment Division, Modeling and Simulation Studies Branch: Seattle, Washington, U.S.A., 1996.
(117) Shaw, D. G.; Reidy, S. K. Chemical and size fractionation of aqueous petroleum dispersions. *Environ. Sci. Technol.* **1979**, *13*, 1259−1263.
(118) Smith, K. E. C.; Thullner, M.; Wick, L. Y.; Harms, H. Dissolved organic carbon enhances the mass transfer of hydrophobic organic compounds from nonaqueous phase liquids (NAPLs) into the aqueous phase. *Environ. Sci. Technol.* **2011**, *45*, 8741−8747.